0013-7227/01/$03.00/0
Printed in U.S.A.

The Journal of Clinical Endocrinology & Metabolism 86(8):3948–3957

Germline RET 634 Mutation Positive MEN 2A-related C-Cell Hyperplasias Have Genetic Features Consistent with Intraepithelial Neoplasia

SALVADOR J. DIAZ-CANO, MANUEL DE MIGUEL, ALFREDO BLANES, ROBERT TASHJIAN, AND HUBERT J. WOLFE

Departments of Pathology, Tufts University–New England Medical Center (S.J.D.-C., R.T., H.J.W.), Boston, Massachusetts 02111; Barts and The London Queen Mary's School of Medicine and Dentistry (S.J.D.-C.), E1 1BB London, United Kingdom; University Hospital of Seville (M.d.M.), 41009-Seville, Spain; and University Hospital of Malaga (A.B.), 29010-Malaga, Spain

C-cell hyperplasias are normally multifocal in multiple endocrine neoplasia type 2A. We compared clonality, microsatellite pattern of tumor suppressor genes, and cellular kinetics of C-cell hyperplasia foci in each thyroid lobe.

We selected 11 females from multiple endocrine neoplasia type 2A kindred treated with thyroidectomy due to hypercalcitoninemia. C-cell hyperplasia foci were microdissected for DNA extraction to analyze the methylation pattern of androgen receptor alleles and microsatellite regions (*TP53*, *RB1*, *WT1*, and *NF1*). Consecutive sections were selected for MIB-1, pRB1, p53, Mdm-2, and $p21^{WAF1}$ immunostaining, DNA content analysis, and *in situ* end labeling. Appropriate tissue controls were run.

Only two patients had medullary thyroid carcinoma foci. Nine informative C-cell hyperplasia patients showed germline point mutation in *RET*, eight of them with the same androgen receptor allele preferentially methylated in both lobes. C-cell hyperplasia foci showed heterogeneous DNA deletions revealed by loss of heterozygosity of *TP53* (12 of 20), *RB1* (6 of 14), and *WT1* (4 of 20) and hypodiploid G_0/G_1 cells (14 of 20), low cellular turnover (MIB-1 index 4.5%, *in situ* end labeling index 0.03%), and significantly high nuclear area to DNA index ratio.

MEN 2A (germline point mutation in *RET* codon 634) C-cell hyperplasias are monoclonal and genetically heterogeneous and show down-regulated apoptosis, findings consistent with an intraepithelial neoplasia. Concordant X-chromosome inactivation and interstitial gene deletions suggest clone expansions of precursors occurring at a point in embryonic development before divergence of each thyroid lobe and may represent a paradigm for other germline mutations. (*J Clin Endocrinol Metab* 86: 3948–3957, 2001)

THE IDENTIFICATION OF *RET* germline mutations in multiple endocrine neoplasia type 2 (MEN 2) has resulted in carrier detection and early diagnosis of C-cell hyperplasias (CCHs) and medullary thyroid carcinomas (MTCs) (1–3). RET mutation seems to be necessary, but other alterations should be required to explain the MEN 2 phenotypic heterogeneity and the differences between CCH and adrenal medullary hyperplasias.

Clonality is still the hallmark of neoplasia and strongly suggests acquired somatic mutations, providing proliferative advantage to a given cell population (4, 5). Clonality has been studied by X-chromosome inactivation (XCI) assays, which are based on the DNA methylation of many genes that render maternal and paternal chromosome functionally nonequivalent (6–8). The same point mutation or single nucleotide polymorphism (SNP) within all cells also implies a common progenitor, (4), and it has been found associated with loss of heterozygosity (LOH) of certain loci (9). LOH should be linked to inactivation of tumor suppressor genes (TSG) by DNA deletions, contributing to tumor cell selection (4). These non-X-linked markers test clonal expansions associated to selective growth advantages (high proliferation and/or abnormally low apoptosis) (4, 10–13), but they fail to identify clones occurring prior to the presence of the genetic lesion (9, 10).

This study investigates the clonal patterns of CCH associated with MEN 2A (*RET* point mutation in codon 634) in both thyroid lobes, based on the analysis of both the methylation pattern of androgen receptor alleles and TSG microsatellite patterns using microdissected tissue samples. The kinetic features of such lesions are also analyzed.

Abbreviations: AR, Androgen receptor; CCH, C cell hyperplasia; HPF, high-power field; ISEL, *in situ* end labeling; LOH, loss of heterozygosity; MEN 2, multiple endocrine neoplasia type 2; MTC, medullary thyroid carcinoma; *NF1*, neurofibromatosis 1; *TP53*, tumor protein p53; *RB1*, retinoblastoma; SNP, single nucleotide polymorphism; TSG, tumor suppressor genes; *WT1*, Wilms' tumor 1; XCI, X-chromosome inactivation.

Materials and Methods

Case selection

MEN 2A kindred with a Cys634 to Tyr substitution of *RET* proto-oncogene (177 members, five generations) were screened for CCH/MTC by basal and pentagastrin-induced calcitonin levels (14–16). All patients fulfilled the clinical and molecular criteria proposed by the International RET Mutation Consortium (17). Patients with pentagastrin-induced hypercalcitoninemia and/or *RET* point mutations underwent total thyroidectomy, the specimens being serially sectioned and completely embedded for histopathologic diagnosis.

Appropriate archival material from both lobes was available from 11 females. We initially selected cases showing 50 or more C cells in at least one ×100 microscope field per lobe (18, 19). C cells were large, mildly to moderately atypical, and confined within the follicular basement membrane, but cytologically indistinguishable from invasive MTC (20, 21). One patient (case CCH-6) did not show *RET* mutation and was

excluded from further analyses. The same areas in consecutive sections were used in each study, and their cellular composition was confirmed in adjacent hematoxylin-eosin-stained sections.

PCR analysis of clonality and TSG microsatellites

One CCH focus containing at least 100 C cells (0.5 mm; Ref. 2) was microdissected from each thyroid lobe (two 20-μm unstained sections/focus). Appropriate controls (follicular cells, lymph node, peripheral nerves, and thyroidal soft tissue) were carried out.

DNA was extracted using a modified phenol-chloroform protocol, (22) and digested with *Hha*I (New England Biolabs, Inc., Beverly, MA). Half of each sample underwent enzymatic digestion (0.8 U/μl), whereas the remaining half was kept as undigested control. Both samples were equally processed, but excluding *Hha*I in the undigested ones (10, 23, 24). A mimicker (0.3 μg of double-stranded and *Xho*I-linearized ϕX174-RII phage) (Life Technologies, Inc., Gaithersburg, MD) was included in each reaction for digestion testing. Complete digestion was checked by gel electrophoresis; incompletely digested samples were phenol chloroform purified and redigested with higher *Hha*I concentration. *Hha*I was then inactivated by phenol-chloroform extraction (22). DNA was precipitated with ice-cold absolute ethanol in the presence of 0.3 mol/liter sodium acetate (pH 5.2) and resuspended in 10 μl of 10 mmol/liter Tris-HCl (pH 8.4), 50 mmol/liter KCl, 1.5 mmol/liter MgCl2, and 100 μg/ml BSA.

The CAG repeat in the first exon of the human androgen receptor (AR) gene was amplified using both digested and undigested DNA templates (13, 23, 25, 26). The undigested DNA was also used for amplification of intron microsatellites at TSG (*TP53*, *RB1*, *WT1*, and *NF1*) loci, according to the optimized conditions shown in Table 1 (25, 27). The tests were run in a Perkin-Elmer thermal cycler model 480 (Perkin-Elmer Corp., Norwalk, CT). The whole PCR volume (10 μl) was electrophoresed into 0.75-mm thick 8% polyacrylamide gels, nondenaturing for the AR product and 20–80% denaturing gradient (from top to bottom) for TSG products (13, 25, 26). The gels were run at 5 V/cm until xylene cyanol band was within the bottom inch of the gel. The gels were then fixed with 7% acetic acid (5 min), dried under vacuum (40 min, 80 C), and put inside a developing cassette containing one intensifying screen and preflashed films (Kodak XAR; Kodak, Rochester, NY) facing the intensifying screen (16–48 h, −70 C). The autoradiograms were developed using an automated processor Kodak-Omat 100 (Kodak).

Only informative cases (balanced allele ratios in undigested and digested controls) were included in the final analysis (10, 11, 13, 25, 26, 28). Allelic imbalance was densitometrically evaluated (EC model 910 optical densitometer; EC Apparatus Co., St Petersburg, FL), considering only allele ratios greater than 4:1 in the normalized digested lanes evidence of monoclonality. Lanes were normalized with their corresponding undigested sample and controls. Only allele ratios greater than 4:1 in any TSG was equally considered evidence of LOH; otherwise, retention of constitutional heterozygosity was assigned. Additional allele bands in the CCH samples not present in the corresponding control were considered evidence of SNP in denaturing gradient gels.

Nuclear DNA quantification by slide cytometry

Feulgen-stained sections were used for densitometric evaluation of DNA content (29). CAS model 200 and the Quantitative DNA Analysis software (Becton Dickinson and Co., Franklin Lakes, NJ) were used for that purpose, measuring at least 200 nuclei (or the whole lesion if smaller) in every CCH focus in the most cellular area until completion in consecutive microscope high power fields (HPFs; ×400). Only complete, nonoverlapping and focused nuclei were quantified in each HPF.

Internal controls (both lymphocytes and histologically normal follicular cells from the same section) were first normalized with complete rat hepatocytes (external controls, one slide/staining holder) (Becton Dickinson and Co.). They were then used for setting the diploid controls and calculating the DNA index of G_0/G_1 cells (≥10% of measured cells with evidence of G_2+M cells) (30). The proliferation rate was calculated from the DNA histogram by subtracting the number of cells within G_0/G_1 limits from the total number of measured cells and expressed as percentage (29, 31). Both mean nuclear area and nuclear area to DNA index ratio of G_0/G_1 cells were recorded. The latter represents a morphometric parameter of apoptosis when coupled with *in situ* end labeling (ISEL) (13, 30). Age- and sex-matched normal thyroids from 10 autopsies were selected for nuclear area and DNA index analysis. At least 1000 C cells were evaluated as controls for this purpose.

ISEL of fragmented DNA

Extensive DNA fragmentation associated with apoptosis was detected by ISEL as previously reported (31–33). Sections were incubated in 2× SSC (20 min, 80 C) and digested with proteinase K [100 μg/ml in Tris-HCl (pH 7.6), 30 min] at room temperature in moist chamber. DNA fragments were digoxigenin-labeled on 5′-protuding termini using the Klenow fragment of *Escherichia coli* DNA polymerase I (1 h at 37 C), detected using antidigoxigenin Fab fragments labeled with alkaline phosphatase, and developed with nitroblue tetrazolium-X phosphate (31–34). Appropriate controls were run, including positive (reactive lymph node), negative (omitting DNA polymerase I), and enzymatic (DNase I digestion before end labeling). The enzymatic controls allowed establishing a reliable positivity threshold in each sample. The ISEL index was expressed as percentage of positive nuclei compared with the total number of C cells in the same HPF (35–37). The whole lesion was screened.

TABLE 1. Primer sequences and PCR cycling conditions for the amplification of polymorphic DNA regions

Primers	Primer sequences	Tandem repeat/PCR product
AR-a[a]	5′-CCGAGGAGCTTTCCAGAATC-3′	CAG repeat/
AR-b[a]	5′-TACGATGGGCTTGGGGAGAA-3′	215–300 bp
p53(1)-a[b]	5′-AGGGATACTATTCAGCCC-3′	CA repeat/
p53(1)-b[b]	5′-ACTGCCACTCCTTGCCCCATTC-3′	103–135 bp
p53(2)-a[b]	5′-GAATCCGGGAGGAGGTTG-3′	AAAAT repeat/
p53(2)-b[b]	5′-AACAGCTCCTTTAATGGCAG-3′	140–175 bp
RB1-a[b]	5′-CTCCTCCCTACTTACTTGT-3′	CTTT(T) repeat/
RB1-b[b]	5′-AATTAACAAGGTGTGGTGGTACACG-3′	266–306 bp
WT1-a[b]	5′-AATGAGACTTACTGGGTGAGG-3′	CA repeat/
WT1-b[b]	5′-TTACACAGTAATTTCAAGCAACGG-3′	~144 bp
NF1-a[b]	5′-CAGAGCAAGACCCTGTCT-3′	CA repeat/
NF1-b[b]	5′-CTCCTAACATTTATTAACCTTA-3′	171–187 bp

All reactions were run in duplicate using 1.5 mM $MgCl_2$ and 1 μl template. A long denaturation (4 min) and expansion (90 sec) were used in the first three cycles for each set of primers.

[a] The AR alleles were amplified using 0.3 μM of each primer and 200 μM of each dNTP (including 7-deaza-dGTP instead of dGTP) (Boehringer-Mannheim, Indianapolis, IN). The amplicon was internally labeled with 0.3 μCi α[^{32}P]-dTTP (800 Ci/mmol, 10 mCi/ml) (New England Nucleotide, Boston, MA). A "hot start" protocol was also used, completing 28 cycles with an annealing temperature of 55° C.

[b] The polymorphic regions of TSG were amplified using 0.25 μM of each primer, 50 μM of each dNTP (Boehringer-Mannheim, Indianapolis, IN), and internally labeled with 0.3 μCi α[^{32}P]-dCTP (3000 Ci/mmol, 10 mCi/ml) (New England Nucleotide, Boston, MA, USA). The annealing temperature was 55° C for all primer sets (except for NF1, it was 52° C), and the number of cycles was experimentally optimized to 26.

Immunohistochemical expression of MIB-1 and cell cycle regulators

After quenching endogenous peroxidase activity with 0.5% H_2O_2-methanol (10 min.), the antigens were retrieved by microwaving sections in 10 mmol/liter citrate buffer (pH 6.0; 750 W, 2 cycles of 5 min) and the sections were transferred to a moist chamber for the remaining steps (34). The tissue sections were incubated overnight at 4 C with the corresponding primary monoclonal antibody (normal pRB1 at 5 μg/ml, abnormal p53 at 1 μg/ml, and cyclin D1, $p21^{WAF1}$, MDM-2, and MIB-1 at 2.5 μg/ml) (Oncogene Science, Inc. and Calbiochem, Cambridge, MA). Nonspecific binding was blocked pretreating the sections with diluted horse serum (1:100) and the signal amplified with biotinylated antimouse secondary antibody (1:200) and peroxidase-labeled avidin-biotin complex (1:100) (Vector Laboratories, Inc., Burlingame, CA). All reactions were developed under microscopic control with 3,3′-diaminobenzidine as chromogen and counterstained with hematoxylin. Appropriate positive (reactive lymph node) and negative (omitting the primary antibody) controls were simultaneously run. The immunohistochemical expression was screened and scored as described for the ISEL analysis.

Statistical analysis of quantitative variables

ANOVA and Student's *t* tests were applied to assess the differences of morphometric features in G_0/G_1 cells by DNA content and considered significant if *P* less than 0.05.

Results

At the time of thyroidectomy, the patients aged 4–8 yr and there was no clinical or laboratory evidence of adrenal or parathyroid pathology. All patients had bilateral CCH, associated with MTC in two cases (CCH-10 and CCH-11). Two cases (four CCH foci) were excluded from the clonality assay. Case CCH-6 showed no germline *RET* mutation and a polyclonal secondary CCH due to chronic thyroiditis (Fig. 1). Case CCH-2 was noninformative due to AR locus LOH (Table 2).

Monoclonal patterns revealed the same inactivated X-chro-

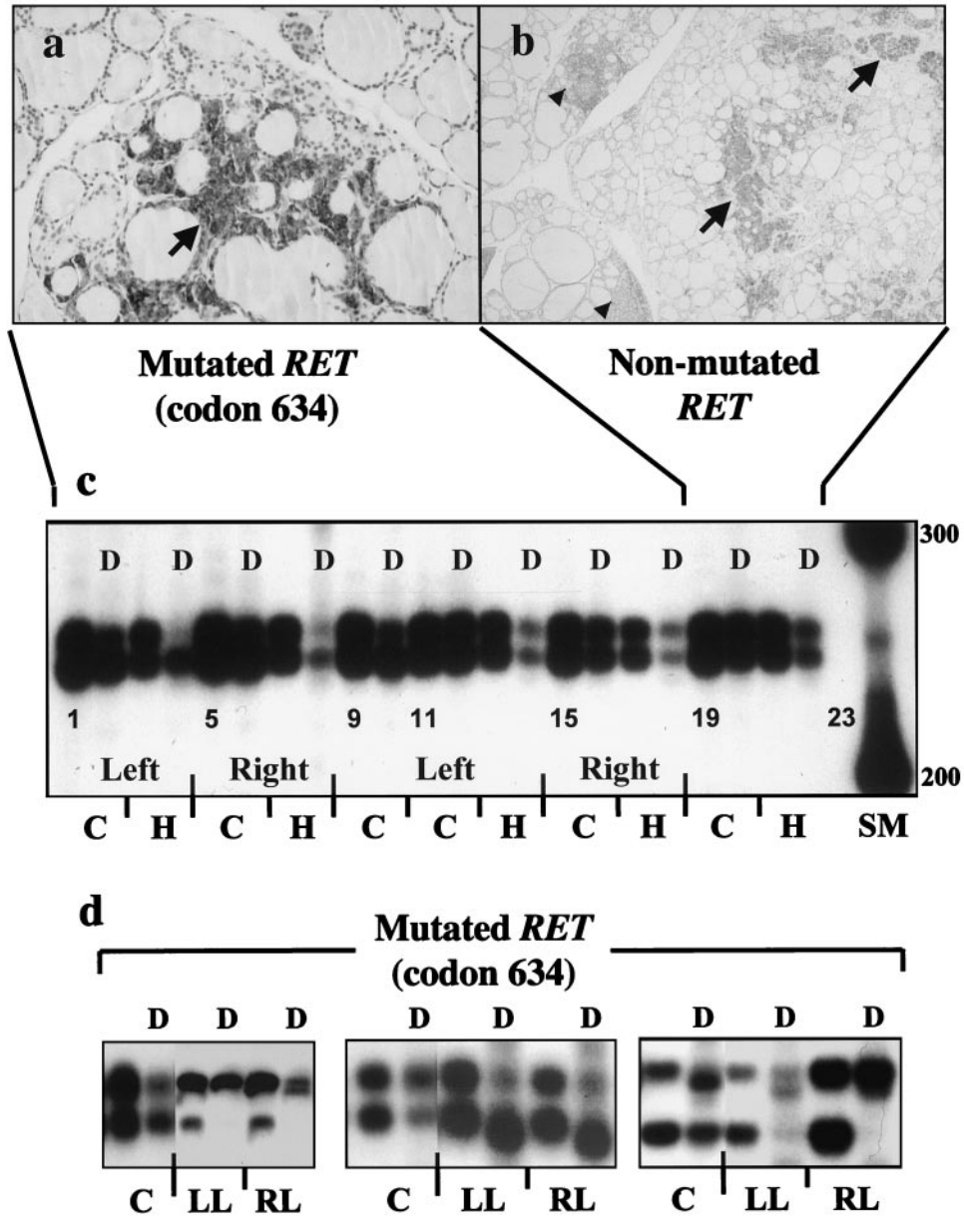

FIG. 1. Allele patterns of androgen receptor and histologic features in CCH. a, Diffuse and nodular growth patterns were observed in CCH associated with MEN-2A and germline mutation of *RET*. The *arrow* points calcitonin-positive C cells (ABC-peroxidase, ×400). b, Diffuse CCH associated with chronic thyroiditis and no germline mutations in codon 634 of RET highlighted by the immunohistochemical demonstration of calcitonin (*arrows*). The lymphocytic infiltrate of chronic thyroiditis (*arrowheads*) is also shown (ABC-peroxidase, ×100). c, Gel patterns in CCH and controls. The *panel* shows monoclonal pattern with the same XCI in both lobes (lanes 1–8, case CCH-1) and polyclonal pattern in a patient with germline point mutation in codon 634 of *RET* (lanes 9–18, case CCH-4) and in a patient with no germline mutation of *RET* (lanes 19–22, case CCH-6). Each case shows undigested and digested (D) lanes of the microdissected sample and its corresponding control. Lane 23 corresponds to the negative control with no template and lane 24 is the size marker (SM). C, Control; H, CCH. d, Three monoclonal patterns in MEN-2A CCH (cases CCH-3, CCH-8, and CCH-11, respectively). The *panel* shows the same X-chromosome inactivated in both thyroid lobes (LL, Left lobe; RL, right lobe) and the balanced methylation of a representative control. The additional band of the larger allele in the digested lane of right lobe (CCH-3) and left lobe (CCH-11) is related with slippage of *Taq* polymerase during the amplification (the sequence corresponded with the amplified locus).

TABLE 2. Analysis of polymorphic DNA regions of AR gene and TSG in CCH foci from patients with MEN-2A and point mutation in codon 634

Sample	Methylation of AR alleles	TP53 (1)	TP53 (2)	RB1	WT1	NF1
CCH1-LL	Unbalanced	LOH-S	ROH	ROH	ROH	ROH
CCH1-RL	Unbalanced	LOH-S	ROH	ROH	ROH	ROH
CCH2-LL[a]	NI-LOH	ROH	ROH	NI	LOH-L	ROH
CCH2-RL[a]	NI-LOH	ROH	ROH	NI	ROH	ROH
CCH3-LL	Unbalanced	NI	ROH	LOH-L	ROH	ROH
CCH3-RL	Unbalanced	NI	ROH	LOH-L	ROH	ROH
CCH4-LL[a]	Balanced	LOH-S	NI	ROH/SNP-SL	ROH	ROH
CCH4-RL[a]	Balanced	LOH-S	NI	ROH	ROH	ROH
CCH5-LL	Unbalanced	LOH-S	ROH	ROH	ROH	ROH
CCH5-RL	Unbalanced	LOH-S	ROH	ROH	ROH	ROH
CCH7-LL[a]	Unbalanced	ROH	ROH	NI	ROH	ROH
CCH7-RL[a]	Unbalanced	ROH	ROH	NI	LOH-S	ROH
CCH8-LL[a]	Unbalanced	LOH-S	ROH	ROH/SNP-L	ROH	ROH
CCH8-RL[a]	Unbalanced	LOH-S	ROH	ROH	ROH	ROH
CCH9-LL	Unbalanced	NI	ROH	LOH-S	ROH	ROH
CCH9-RL	Unbalanced	NI	ROH	LOH-S	ROH	ROH
CCH10-LL[b]	Unbalanced	LOH-S	NI	NI	ROH	NI
CCH10-RL[b]	Unbalanced	LOH-S	NI	NI	ROH	NI
CCH11-LL[b]	Unbalanced	LOH-L	NI	ROH	ROH	NI
CCH11-RL[b]	Unbalanced	LOH-L	NI	ROH	ROH	NI

ROH, Retention of heterozygosity; LL, left lobe; RL, right lobe; L, larger allele; S, smaller allele; NI, noninformative.
[a] Cases CCH-2, -4, -7, and -8 revealed genetic heterogeneity in left and right lobes.
[b] Cases CCH-10 and CCH-11 revealed coexistent medullary thyroid carcinoma. Case CCH-6 showed no *RET* point mutations in codon 634.

mosome in both lobes from a given patient, showing either the larger allele (two cases, 4 CCH foci) or the smaller allele preferentially methylated (six cases, 12 CCH foci; Fig. 1). Another patient (two CCH foci) displayed a polyclonal pattern. Assuming equal probability of methylation of each AR allele at the cellular level, the probability of concordant methylation patterns of AR alleles will be 0.5 (Fig. 2a). However, tissues from informative females can be polyclonal, monoclonal with preferential methylation of the larger allele, or monoclonal with the smaller allele predominating (Fig. 2b) (38). Under those circumstances and assuming independent methylation of each allele, equal *a priori* probability should be expected for each chance and tissue ($P = 1/3$). In tissue comparisons from informative patients (two different alleles present), concordant allele patterns would expected in $2(1/3)^n$, being 2 = number of alleles and n = number of lesions compared. Therefore, identical patterns could be randomly found in $2(1/3)^2 = 0.22$ when two tissue samples are compared (Fig. 2b). Therefore, the probability of randomly finding identical allele patterns in tissues from eight females would be $0.22^8 = 5.49\ 10^{-6}$. Any tissue-specific variability in DNA methylation was excluded using multiple matched controls of the same sample size. The polyclonal case (CCH-4, Table 2) could not be accurately assessed for this purpose, due to the absence of gel pattern differences between true polyclonal proliferation and proliferation of two clones revealing different X chromosome inactivated (Fig. 2b).

All cases showed genetic abnormality in at least one TSG locus, especially *TP53* LOH (Table 2). LOH/SNP analyses showed *TP53* abnormalities in 6 of 10 informative cases (12 of 20 CCH foci, 60%), *RB1* alterations in 4 of 7 informative patients (6 of 14 CCH foci, 43%), and *WT1* deletions in 2 of 10 informative patients (2 of 20 CCH foci, 10%) (Table 2, Fig. 3). No alterations were detected in *NF1* locus. *TP53* abnormalities were concordantly detected in both lobes in all patients in at least one polymorphic region. Discordant genetic results were observed only in two patients for *RB1* (SNP) and in two patients for *WT1* (LOH), and coexistent *TP53* and *RB1* genetic alterations in two patients (Table 2).

The DNA content analysis revealed diploid G_0/G_1 cells in all cases, hypodiploid G_0/G_1 cells (DNA index < 0.9) in 14 of 20 (70%) CCH foci, and hyperdiploid G_0/G_1 cells ($1.15 <$ DNA index < 1.85) in 1 of 20 (5%) CCH foci (Table 3). Hypodiploid G_0/G_1 cells revealed a relatively decreased nuclear area (35.11 ± 4.20 μm (2) and a significantly higher nuclear area to DNA index ratio [43.12 ± 3.59 μm (2), $P < 0.003$) than control C cells [36.48 ± 3.98 μm (2), 37.22 ± 4.06 μm^2, respectively]. Low proliferation indices were obtained from the DNA histogram analysis (<5% for monoclonal foci and 7.6–8.3% for polyclonal foci). MIB-1 and cell cycle regulator immunoexpressions and ISEL revealed a heterogeneous marker distribution (Fig. 4). Both proliferation and apoptosis indices were low, especially the ISEL index (Table 3). Remarkably, no p53 expression was detected in CCH foci (Fig. 4).

Discussion

CCHs in MEN 2A patients were found monoclonal and showed the same inactivated X-chromosome in both lobes and multiple TSG abnormalities. These findings and the down-regulation of apoptosis are consistent with an intraepithelial neoplasia and suggest that progressional genetic events occur early in thyroid development.

The same AR allele was preferentially methylated in both lobes in monoclonal CCHs (eight of nine informative patients, 89%; Table 2), suggesting that a common progenitor contributed to those lesions (25, 39, 40), and support a neoplastic nature. These concordant patterns also support a clonal expansion of C-cell precursors between the random XCI and the precursor migration into the thyroid anlage (~15

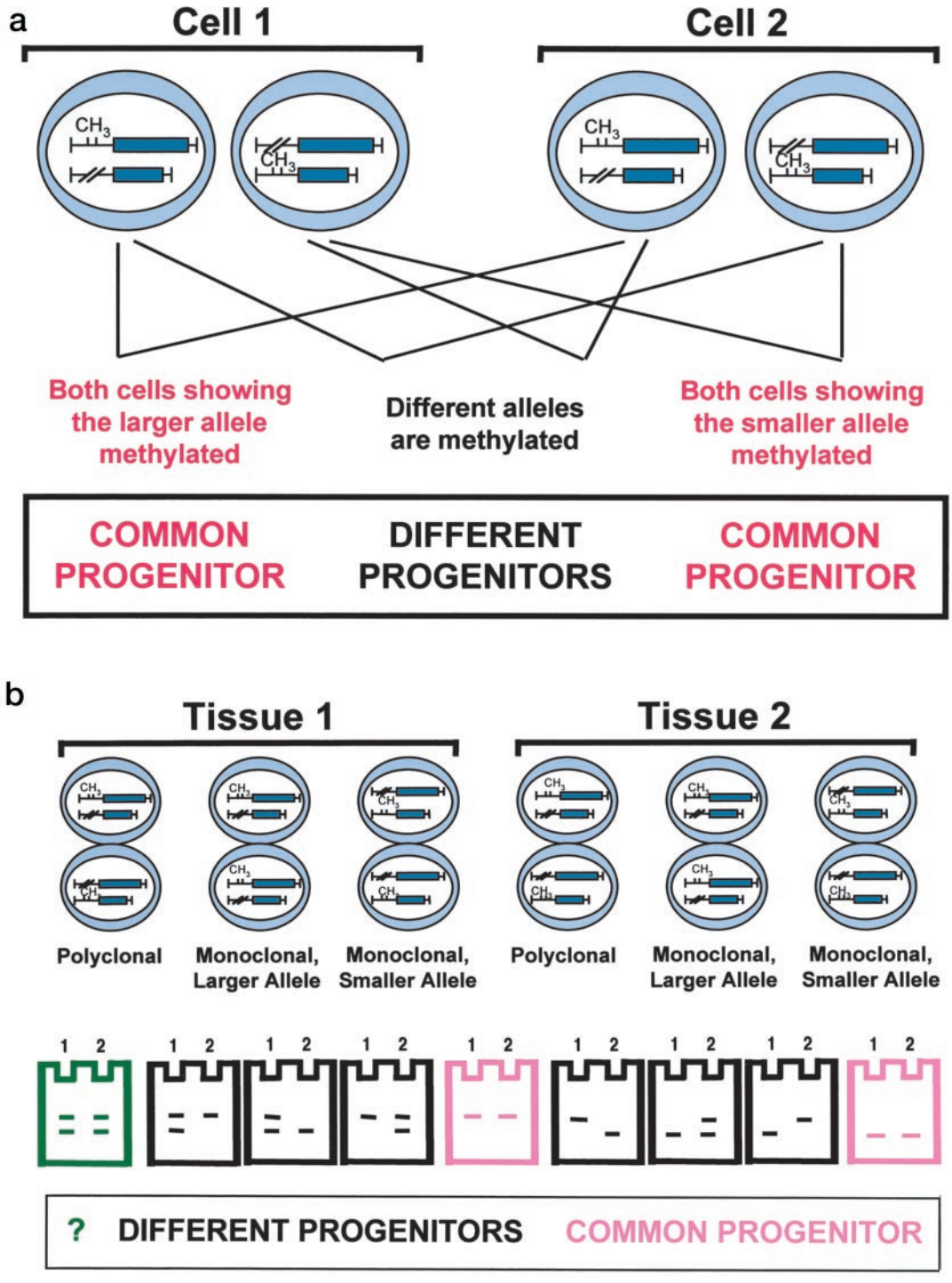

FIG. 2. Comparison of XCI patterns. Only the active and nonmethylated androgen receptor allele is expressed in a given cell, and can be distinguished by the length of the polymorphic marker in the exon 1 in informative patients. However, comparative analyses give different possibilities at the cellular and tissue levels. a, The cell-cell comparison shows four potential possibilities, two revealing different X-chromosomes inactivated and suggesting different progenitors (50%), and other two displaying the same X-chromosome inactivated (either the larger allele or the smaller allele, 50%), consistent with common progenitor. b, Three possibilities can be found at the tissue level, depending on the inactivation of only one allele in monoclonal tissues (the larger or the smaller one) or both alleles in polyclonal tissues. The comparison of two given tissues (1 and 2) would then result in nine theoretical options (each one represented in different gels); only two of them are consistent with a common progenitor contributing the cells, both tissues expressing either the larger or the smaller allele (*pink*). If random inactivation of both alleles is present (*green*), no clonality assessment can be achieved because the progenitor cell can be either common or different. The remaining cases (*black*) represent tissue development from different progenitors.

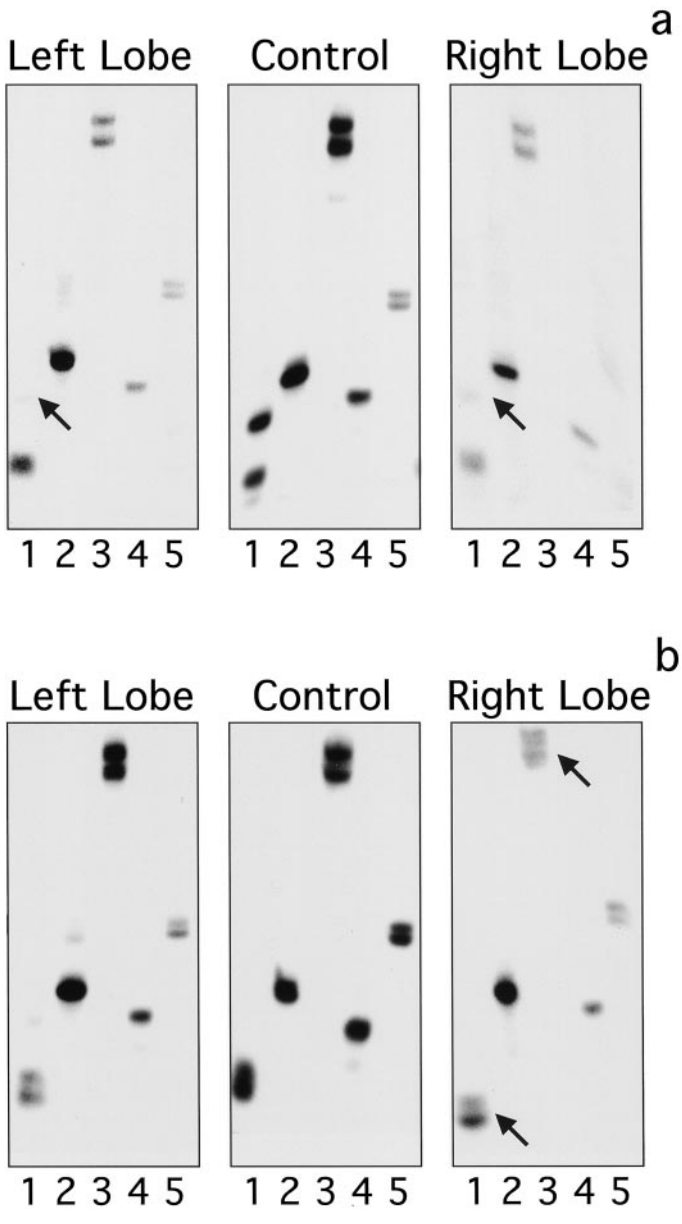

FIG. 3. Microsatellite analysis of tumor suppressor genes (1, TP53 (1); 2, TP53 (2); 3, RB1; 4, WT1; 5, NF1) in CCH. LOH or SNP was detected in polymorphic DNA regions of tumor suppressor genes. The *arrows* point to the heterogeneous genetic lesions in TP53 (LOH; a and b) and RB1 (SNP; b) observed.

wk, Fig. 5) (11, 41). Supporting this point, patients of these kindred also revealed concordant monoclonal patterns in 90% nodules from adrenal medullary hyperplasias and microsatellite abnormalities in at least one TSG in 75% pheochromocytomas (26, 42). Early clonal expansions in neural crest derivatives could explain those findings, but other alternative explanations for the monoclonal pattern must be excluded.

The first issue to consider is the patch size concept or contiguous cellular regions of the same lineage (10, 11, 13, 25). The mosaic patch size could be the cause of monoclonal patterns in small samples, but it would not explain the concordant pattern in both lobes, especially with samples including at least 100 cells (10, 38, 43). In addition, technical aspects such as PCR bias against the larger allele could contribute to preferential amplification of the smaller allele. Our DNA extraction protocol included a long protein digestion and retrieved DNA of ~1 kb (data not shown), excluding degraded DNA as cause (13, 22, 25, 28, 44). Our PCR design also included long denaturation and extension in the first three cycles and 7-deaza-dGTP in the amplification mixture to avoid defective amplification of CG-rich sequences (Table 1) (10, 13, 24, 25, 40). These technical considerations could reasonably exclude the PCR bias as cause of concordant monoclonal patterns, as revealed by the two cases showing the larger allele methylated (Fig. 1).

The polyclonal pattern in patients with germline *RET* mutation (CCH-4) needs some considerations. XCI assays can result in polyclonal patterns if the restriction endonuclease digestion is incomplete or the target DNA is hypermethylated (10, 11, 13, 25, 28). Suboptimal enzymatic digestion may change the clonality pattern of monoclonal tissues (10, 28), but that possibility was excluded keeping internal controls of endonuclease digestion. Although some DNA denaturation must be expected during embedding and extraction, both the long digestion (16 h) and the *Hha*I activity on single-stranded DNA assure complete digestion. Repeated polyclonal patterns were obtained using nonboiled templates. We are currently testing methylation in these lesions. Likewise, any significant contamination can explain polyclonal results as those reported in MEN 2 MTC (45), opposed to the clonal origin previously reported in inherited MTC and pheochromocytomas (46, 47). Contamination was excluded by careful microdissection under microscopic control and multiple sampling (10, 11). Finally, the coexistence of *TP53* and *RB1* abnormalities (Table 2) support a neoplastic nature and agrees with the high MTC incidence (60%) in double heterozygous animals for *TP53* and *RB1* (48). In this scenario, the polyclonal pattern could be the result of either C-cell precursor expansions before the random XCI or clonal proliferation of cells showing different inactivated X-chromosome (Fig. 5) (11, 45).

The inherited genetic defect can determine an accelerated process of somatic alterations and DNA deletions (hypodiploid G_0/G_1 cells and TSG-LOH) (11, 13), favoring cellular heterogeneity and molecular progression (11, 25). Our results suggest that progression in CCHs involves multiple genes, especially *TP53* and *RB1* as reported in MTC (48, 49). Although the number of cases is not sufficient to exclude chance, the concordant *TP53* deletion found in three patients (Table 2) suggests that *TP53* deletions have occurred at a point in embryonic development before divergence of the C-cell precursors of each thyroid lobe in this patient subset. Therefore, these mutations should occur earlier than previously thought and correlate with the clinical detection of MTC in patients younger than 5 yr. Conversely, the heterogeneity of *RB1* and *WT1* alterations and intragenetic polymorphism of *TP53* mutations support their somatic nature and a sort of "hot spot" for such mutations. *WT1* and *RET* have already shown collaborative effects, as revealed by the presence of genitourinary abnormalities in *RET* or *GDNF* knockout mice (50, 51). In contrast, no patient in this series showed *NF1* alterations, although this locus has revealed

TABLE 3. Results of DNA-Ploidy, MIB-1, and cell cycle regulator immunoexpression, and ISEL in CCH from MEN-2A patients with point mutation in codon 634[a]

Case no.	DNA-Ploidy	MIB-1 (%)	MDM2 (%)	pRB (%)	$p21^{WAF1}$ (%)	ISEL (%)
CCH-1	Hypodiploid	3.1	4.2	4.8	1.4	0.03
CCH-2	Hypodiploid	2.5	6.2	4.0	2.1	0.05
CCH-3	Hypodiploid	2.1	4.3	4.3	1.7	0.03
CCH-4	Hypodiploid	3.7	5.5	5.1	1.7	0.04
CCH-5	Diploid	6.8	5.6	4.6	1.6	0.02
CCH-7	Diploid	5.9	3.1	7.0	1.4	0.03
CCH-8	Hypodiploid	4.3	3.2	8.7	1.2	0.01
CCH-9	Hypodiploid	4.6	3.0	8.1	1.2	0.02
CCH-10[b]	Hypodiploid	4.3	4.6	5.9	1.5	0.03
CCH-11[b]	Hypodiploid	4.5	4.4	6.6	1.5	0.02
Av ± SD		4.18 ± 1.44	4.41 ± 1.11	5.91 ± 1.64	1.53 ± 0.27	0.03 ± 0.01

[a] These scores show the combined results CCH areas from both lobes in each patient because of the small size that avoid to screen 50 HPF/CCH focus.

[b] Cases CCH-10 and CCH-11 showed coexistent MTC foci (excluded in the screening). Case CCH-6 did not show *RET* point mutations in codon 634.

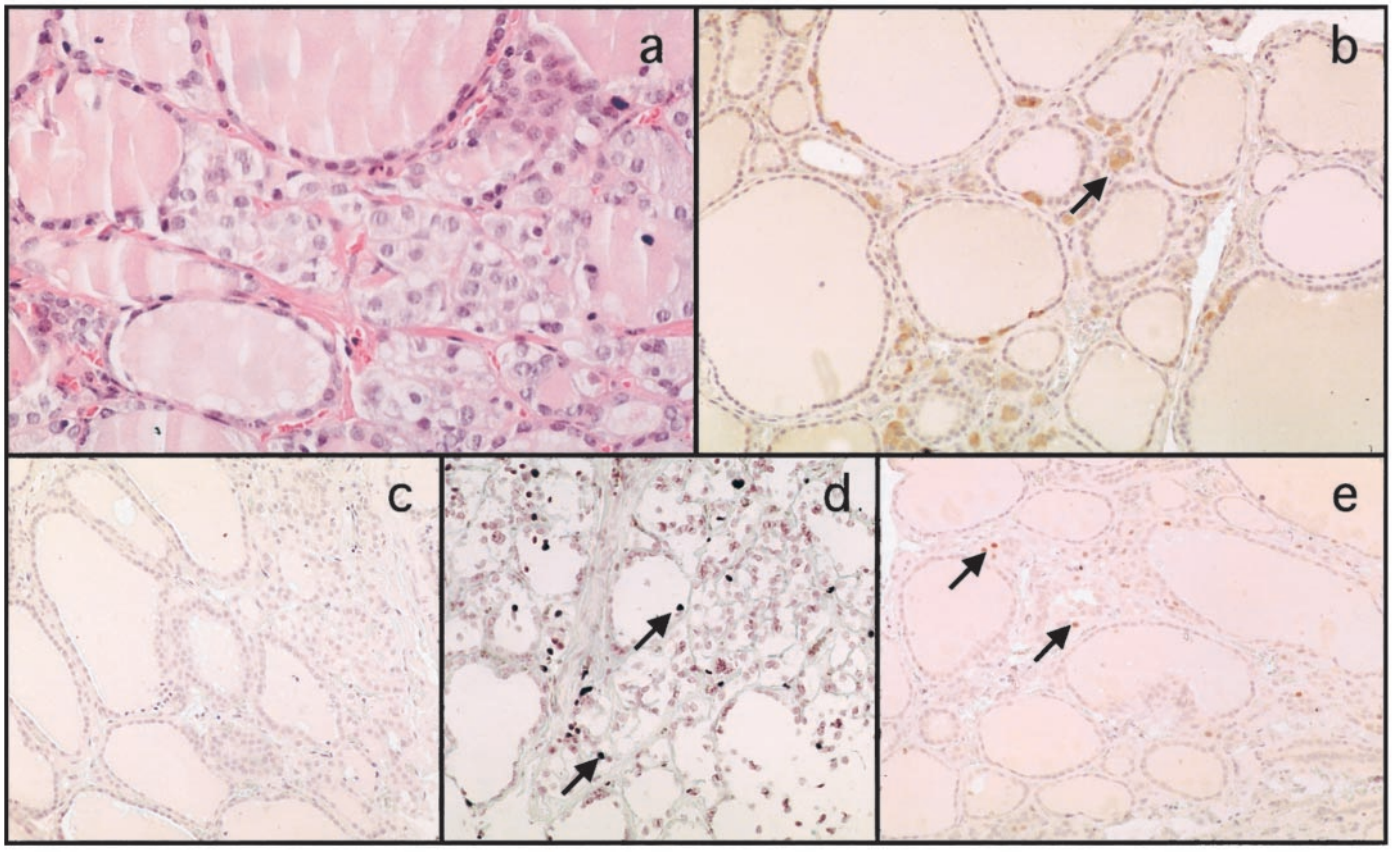

FIG. 4. Immunohistochemistry and ISEL in CCHs. C cells show cytoplasmic MIB-1 staining (b) along with relatively low nuclear $p21^{WAF1}$ labeling (e) and ISEL index (d). c, No abnormal p53 immunostaining was detected. (a, H&E, ×400; b, c, and e, ABC-peroxidase and 3,3′-diaminobenzidine, ×100; d, digoxigenin end labeling developed with alkaline phosphatase and NBT-X phosphate, ×100). The *arrows* point to positive signal.

alterations in neural crest tumors (especially pheochromocytomas) (52, 53). Early clonal expansions in neural crest derivatives accumulating genetic alterations would be the expression of multistep tumorigenesis and is also supported by the reported abnormalities of loci on chromosomes 1 and 3 (54, 55). The presence of additional somatic *RET* mutations has been reported in MTC and should be considered expression of genetic progression and tumor cell selection rather than evidence against the clonality of those lesions (54). Another aspect to consider is the origin of all patients from a single family and the influence of familial effects on the results. However, the familial genetic background cannot explain the association of unrelated aspects such as concordant patterns of clonality and the presence of multiple TSG abnormalities.

A *TP53*- and *RB1*-knockout model revealed MTC within the first 9–15 months of mouse life (60–83%) with the highest incidence in double heterozygous animals (mutated *RB1* and

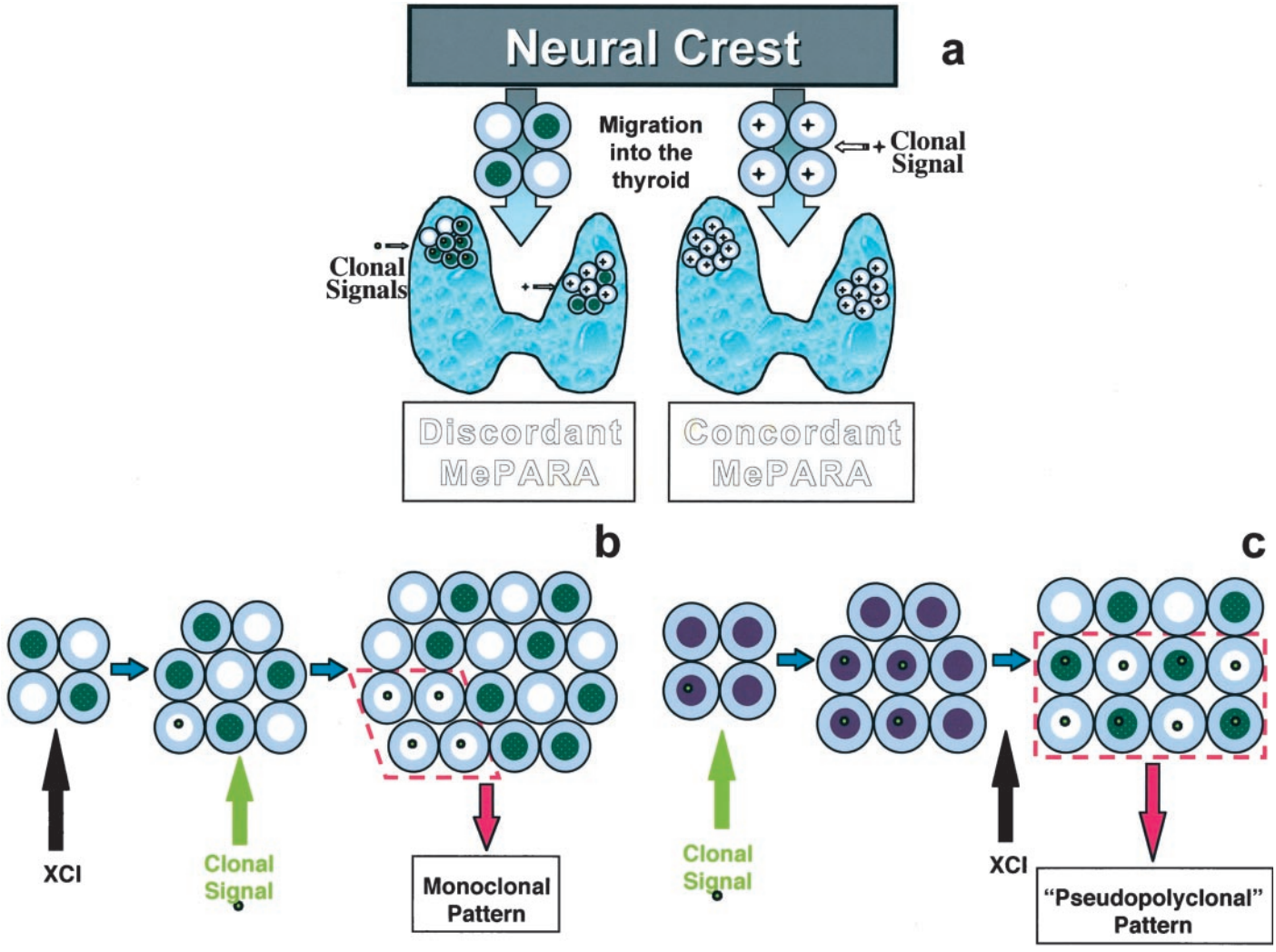

FIG. 5. a, Relative timing of clonal expansion of C cells and the location of C-cell precursors in the thyroid anlage Clonal Signal and expansion of C cells after locating in the thyroid would make unlikely cells showing the same allele methylated (*left*). The opposite scenario should be considered for consistently concordant methylation pattern of androgen receptor alleles (MePARA): clonal signal and expansions should happen before the location of C-cell precursors in the thyroid (*right*). b and c, Relative timing of clonal expansion of C cells and XCI. b, Monoclonal proliferation requires an already established inactivation of the X chromosome before the clonal expansion to result in monoclonal gel pattern. c, If the clonal signal and expansion antecedes the XCI, selected cells can potentially inactivate any of the alleles and show a "pseudopolyclonal" gel pattern.

TP53) (48). The absence of normal *TP53* function would protect tumor cells from apoptosis (56) and contributes to an increased *RB1* mutation rate in advanced tumors (48). Remarkably low ISEL indices and low-to-normal proliferation indices were observed in this CCH series. The reduced cellular loss associated with longer survival of initiated/mutated cells would promote progression from preinvasive stages over an extended period of time (11, 13, 57), and genetic instability (49). Transforming mutations that escape cell repair systems will accumulate and promote early preneoplastic foci only after inhibiting apoptosis (11, 13, 58). The postmitotic repairing systems are less effective in low-proliferation lesions (59), explaining the presence of heterogeneous and nonrandomly distributed mutations (60). In contrast, high proliferation and mutation rates determine homogeneous DNA damage and activation of apoptosis (57, 60, 61). Normal pRB1 and low $p21^{WAF1}$ expressions found in this series are consistent with low proliferation and apoptotic indices. Only higher proliferation rates and increased $p21^{WAF1}$ would inactivate pRB1 resulting in higher apoptosis (59). The combined delivery of two cooperative genes, like $p21^{WAF1}$ and *TP53*, would lead the cyclin D/CDK-pRB1 pathway toward growth arrest and apoptosis (62, 63).

Some clinically relevant topic still remains unknown. *RET* encodes a receptor tyrosine kinase that is expressed in neural crest derivatives and their corresponding tumors, MTC, and pheochromocytoma (64). RET mutations of codon 634 cause receptor dimerization and constitutively activate the tyrosine kinase (65), thereby mimicking the effect caused by the binding of a ligand to the receptor. In general, a single mutation causing a neoplasm is unlikely, and other genetic alterations (*TP53* and *RB1* in this series) would be required (11). Although normal tissues are heterogeneous and show random LOH and DNA deletions in 4–20% (66–68), that level of

somatic genetic alterations cannot explain this series incidence of TSG abnormalities, especially for CCH foci with alterations in two loci (CCH-4 and CCH-8). Similarly, somatic missense mutations at codon 918 of *RET* have been reported in 20% MTC and in a sample of CCH from MEN 2 patients (54). These factors and the preexisting germline mutation of *RET* may contribute to C-cell tumorigenesis. Those findings suggest that CCHs in MEN 2A are intraepithelial neoplasias.

In conclusion, genetic (monoclonal proliferation with multiple TSG abnormalities) and kinetic (down-regulated apoptosis) evidences suggest that MEN 2A CCHs are intraepithelial neoplasias. Concordant XCI pattens in both lobes support early clone expansions preceding divergence of C-cell precursors of each thyroid lobe; this may represent a paradigm for other germline mutations during embryogenesis.

Acknowledgments

Received April 12, 2000. Accepted April 2, 2001.

Address all correspondence and requests for reprints to: Salvador J. Diaz-Cano, M.D., Ph.D., Department of Histopathology and Morbid Anatomy, The Royal London Hospital, Whitechapel, London E1 1BB, United Kingdom. E-mail: s.j.diaz-cano@mds.qmw.ac.uk.

This work was presented in part as abstract forms at the United States and Canadian Academy of Pathology (USCAP) Meetings in Orlando, Florida (March 1997), and Boston, Massachusetts (February 1998). This work was performed at the Departments of Pathology, Tufts University–New England Medical Center (Boston, MA) and St. Bartholomew's and the London NHS Trust (London, UK).

References

1. **Santoro M, Carlomagno F, Romano A, et al.** 1995 Activation of *RET* as a dominant transforming gene by germline mutations of MEN2A and MEN 2B. Science 267:381–383
2. **Mulligan LM, Kwok JB, Healey CS, et al.** 1993 Germ-line mutations of the RET proto-oncogene in multiple endocrine neoplasia type 2A. Nature 363:458–460
3. **Lips CJ, Landsvater RM, Hoppener JW, et al.** 1994 Clinical screening as compared with DNA analysis in families with multiple endocrine neoplasia type 2A. N Engl J Med 331:828–835
4. **Nowell PC** 1976 The clonal evolution of tumor cell populations. Science 194: 23–28
5. **Fialkow PJ** 1976 Clonal origin of human tumors. Biochim Biophys Acta 458: 283–321
6. **Kappler JW** 1971 The 5-methylcytosine content of DNA: tissue specificity. J Cell Physiol 78:33–36
7. **Laird PW, Jaenish R** 1994 DNA methylation and cancer. Hum Mol Genet 3:1487–1495
8. **Lyon MF** 1992 Some milestones in the history of X-chromosome inactivation. Annu Rev Genet 26:17–28
9. **Sternlicht M, Mirell C, Safarians S, Barsky SH** 1994 A novel strategy for the investigation of clonality in precancerous disease states and early stages of tumor progression. Biochem Biophys Res Commun 199:511–518
10. **Diaz-Cano SJ, Blanes A, Wolfe HJ** 2001 PCR techniques for clonality assays. Diagn Mol Pathol 10:24–33
11. **Diaz-Cano SJ** 1998 Clonality studies in the analysis of adrenal medullary proliferations: Application principles and limitations. Endocr Pathol 9:301–316
12. **Salomon RN, Diaz-Cano S** 1995 Introduction to apoptosis. Diagn Mol Pathol 4:235–238
13. **Diaz-Cano SJ, de Miguel M, Blanes A, Tashjian R, Galera H, Wolfe HJ** 2000 Clonality as expression of distinctive cell kinetics patterns in nodular hyperplasias and adenomas of the adrenal cortex. Am J Pathol 156:311–319
14. **Graze K, Spiler IJ, Tashjian AH, Jr, et al.** 1978 Natural history of familial medullary thyroid carcinoma: effect of a program for early diagnosis. N Engl J Med 299:980–985
15. **Gagel RF, Tashjian Jr AH, Cummings T, et al.** 1988 The clinical outcome of prospective screening for multiple endocrine neoplasia type 2 a: an 18 year experience. N Engl J Med 318:478–485
16. **Gagel RF, Cote GJ, Martins Bugalho MJ, et al.** 1995 Clinical use of molecular information in the management of multiple endocrine neoplasia type 2A. J Intern Med 238:333–341
17. **Eng C, Clayton D, Schuffenecker I, et al.** 1996 The relationship between specific RET proto-oncogene mutations and disease phenotype in multiple endocrine neoplasia type 2. International RET mutation consortium analysis. JAMA 276:1575–1579
18. **Wolfe HJ, Melvin KE, Cervi-Skinner SJ, et al.** 1973 C-cell hyperplasia preceding medullary thyroid carcinoma. N Engl J Med 289:437–441
19. **Biddinger PW, Ray M** 1993 Distribution of C cells in the normal and diseased thyroid gland. Pathol Annu 28 :205–229
20. **Perry A, Molberg K, Albores-Saavedra J** 1996 Physiologic versus neoplastic C-cell hyperplasia of the thyroid: separation of distinct histologic and biologic entities. Cancer 77:750–756
21. **McDermott MB, Swanson PE, Wick MR** 1995 Immunostains for collagen type IV discriminate between C-cell hyperplasia and microscopic medullary carcinoma in multiple endocrine neoplasia, type 2a. Hum Pathol 26:1308–1312
22. **Diaz-Cano SJ, Brady SP** 1997 DNA extraction from formalin-fixed paraffin-embedded tissues: protein digestion as a limiting step for retrieval of high quality DNA. Diagn Mol Pathol 6:342–346
23. **Mutter GL, Chaponot ML, Fletcher JA** 1995 A polymerase chain reation assay for non-random X chromosome identifies monoclonal endometrial cancer and precancers. Am J Pathol 146:501–508
24. **Mutter GL, Boynton KA** 1995 PCR bias in amplification of AR alleles, a trinucleotide repeat marker used in clonality studies. Nucleic Acids Res 23: 1411–1418
25. **Diaz-Cano SJ, Blanes A, Rubio J, Matilla A, Wolfe HJ** 2000 Molecular evolution and intratumor heterogeneity by topographic compartments in muscle-invasive transitional cell carcinoma of the urinary bladder. Lab Invest 80: 279–289
26. **Diaz-Cano SJ, de Miguel M, Blanes A, Tashjian R, Galera H, Wolfe HJ** 192 2000 Clonal patterns in phaechromocytomas and MEN-2A adrenal medullary hyperplasias: histologic and kinetic correlates. J Pathol 192:221–228
27. **Cawkwell L, Bell SM, Lewis FA, Dixon MF, Taylor GR, Quirke P** 1993 Rapid detection of allele loss in colorectal tumours using microsatellites and fluorescent DNA technology. Br J Cancer 67:1262–1267
28. **Diaz-Cano SJ** 2000 Designing a molecular analysis of clonality in tumours. J Pathol 191:343–344
29. **Bibbo M, Bartels PH, Dytch HE, Wied GL** 1991 Cell image analysis. In: Bibbo M, ed. Comprehensive cytopathology. Philadelphia: W.B. Saunders Co.; 965–983
30. **Sherwood SW, Schimke RT** 1995 Cell cycle analysis of apoptosis using flow cytometry. In: Schwartz LM, Osborne BA, eds. Cell death. San Diego: Academic Press; 77–97
31. **Koch M, de Miguel M, Höfler H, Diaz-Cano SJ** 2000 Kinetic profiles of intraepithelial and invasive prostatic neoplasias: the key role of down-regulated apoptosis in tumor progression. Virchows Arch 436:413–420
32. **Wijsman JH, Jonker RR, Keijzer R, van de Velde CJH, Cornelisse CJ, van Dierendonck JH** 1993 A new method to detect apoptosis in paraffin sections: In situ end-labeling of fragmented DNA. J Histochem Cytochem 41:7–12
33. **Diaz-Cano SJ, Garcia-Moliner M, Carney W, Wolfe HJ** 1997 Bcl-2 expression and DNA fragmentation in breast carcinoma, pathologic and steroid hormone receptors correlates. Diagn Mol Pathol 6:199–208
34. **Taylor CR, Cote RJ** 1994 Immunomicroscopy: a diagnostic tool for the surgical pathologists. Philadelphia: W.B. Saunders Co
35. **Simpson JF, Dutt PL, Page DL** 1992 Expression of mitosis per thousand cells and cell density in breast carcinomas. A proposal. Hum Pathol 23:608–611
36. **Diaz-Cano SJ, Leon MM, de Miguel M, Galera-Davidson H, Wolfe HJ** 1996 Mitotic index quantification: different approaches and their value in adrenal cortical proliferative lesions. Lab Invest 74:170A
37. **Harjacek M, Diaz-Cano S, Alman BA, et al.** 2000 Prominent expression of mRNA for proinflammatory cytokines in synovium in patients with juvenile rheumatoid arthritis or chronic lyme arthritis. J Rheumatol 27:497–503
38. **Diaz-Cano SJ, Wolfe HJ** 1997 Clonality in Kaposi's sarcoma [Letter; comment]. N Engl J Med 337:571–572
39. **Quade BJ, McLachlin CM, Soto-Wright V, Zuckerman J, Mutter GL, Morton CC** 1997 Disseminated peritoneal leiomyomatosis. Clonality analysis by X chromosome inactivation and cytogenetics of a clinically benign smooth muscle proliferation. Am J Pathol 150:2153–2166
40. **Alman BA, Pajerski ME, Diaz-Cano S, Corboy K, Wolfe HJ** 1997 Aggressive fibromatosis (desmoid tumor) is a monoclonal disorder. Diagn Mol Pathol 6:98–101
41. **Sugiyama S** 1969 Embryonic development of human thyroid gland and ultimobranchial body. Acta Endocr 179(Suppl 138):179
42. **Diaz-Cano SJ, Blanes A** 1999 Influence of intratumour heterogeneity in the interpretation of marker results in phaeochromocytomas. J Pathol 189:627–628
43. **Gale RE, Wheadon H, Boulos P, Linch DC** 1994 Tissue specificity of X-chromosome inactivation patterns. Blood 83:2899–2905
44. **Brady SP, Magro CM, Diaz-Cano SJ, Wolfe HJ** 1999 Analysis of clonality of atypical cutaneous lymphoid infiltrates associated with drug therapy by PCR/DGGE. Hum Pathol 30:130–136
45. **Ferraris AM, Mangerini R, Gaetani GF, Romei C, Pinchera A, Pacini F** 1997 Polyclonal origin of medullary carcinoma of the thyroid in multiple endocrine neoplasia type 2. Hum Genet 99:202–205

46. **Baylin SB, Gann DS, Hsu SH** 1976 Clonal origin of inherited medullary thyroid carcinoma and pheochromocytoma. Science 193:321–323
47. **Baylin SB, Hsu SH, Gann DS, Smallridge RC, Wells SA** 1978 Inherited medullary thyroid carcinoma: a final monoclonal mutation in one of multiple clones of susceptible cells. Science 199:429–431
48. **Williams BO, Remington L, Albert DM, Mukai S, Bronson RT, Jacks T** 1994 Cooperative tumorigenic effects of germline mutations in Rb and p53. Nat Genet 7:480–484
49. **Wang DG, Liu WH, Johnston CF, Sloan JM, Buchanan KD** 1998 Bcl-2 and c-Myc, but not bax and p53, are expressed during human medullary thyroid tumorigenesis. Am J Pathol 152:1407–1413
50. **Shefelbine SE, Khorana S, Schultz PN, et al.** 1998 Mutational analysis of the GDNF/RET-GDNFR α signaling complex in a kindred with vesicoureteral reflux. Hum Genet 102:474–478
51. **Schedl A, Hastie ND** 2000 Cross-talk in kidney development. Curr Opin Genet Dev 10:543–549
52. **Calender A** 2000 Molecular genetics of neuroendocrine tumors. Digestion 62:3–18
53. **Nakamura T** 1995 Genetic markers and animal models of neurocristopathy. Histol Histopathol 10:747–759
54. **Marsh DJ, Andrew SD, Eng C, et al.** 1996 Germline and somatic mutations in an oncogene: RET mutations in inherited medullary thyroid carcinoma. Cancer Res 56:1241–1243
55. **Eng C, Mulligan LM, Healey CS, et al.** 1996 Heterogeneous mutation of the RET proto-oncogene in subpopulations of medullary thyroid carcinoma. Cancer Res 56:2167–2170
56. **Howes KA, Ransom N, Papermaster DS, Lasudry JGH, Albert DM, Windle JJ** 1994 Apoptosis or retinoblastoma: Alternative fates of photoreceptors expressing the HPV-16 E7 gene in the presence or absence of p53. Genes Dev 8:1300–1310
57. **Simpson AJG** 1997 The natural somatic mutation frequency and human carcinogenesis. Adv Cancer Res 71:209–240
58. **Ames BN, Shinega MK, Gold LS** 1993 DNA lesions, inducible DNA repair, and cell division: three key factors in mutagenesis and carcinogenesis. Environ Health Perspect 101(Suppl 5):35–44
59. **Cordon-Cardo C** 1995 Mutation of cell cycle regulators. Biological and clinical implications for human neoplasia. Am J Pathol 147:545–560
60. **Li ZH, Aaltonen LA, Shu Q, Srivastava S, Grizzle WE, Shibata D** 1996 Effects of mutation and growth rates on patterns of microsatellite instability. Am J Pathol 148:1757–1761
61. **Farber E** 1995 Cell proliferation as a major risk factor for cancer: a concept of doubtful validity. Cancer Res 55:3759–3762
62. **Sandig V, Brand K, Herwig S, Lukas J, Bartek J, Strauss M** 1997 Adenovirally transferred p16INK4/CDKN2 and p53 genes cooperate to induce apoptotic tumor cell death. Nat Med 3:313- 319
63. **Canman CE, Gilmer TM, Coutts SB, Kastan MB** 1995 Growth factor modulation of p53-mediated growth arrest versus apoptosis. Genes Dev 9:600–611
64. **Nakamura T, Ishizaka Y, Nagao M, Hara M, Ishikawa T** 1994 Expression of the ret proto-oncogene product in human normal and neoplastic tissues of neural crest origin. J Pathol 172:255–260
65. **Santoro M, Carlomagno F, Romano A, et al.** 1995 Activation of RET as a dominant transforming gene by germline mutations of MEN2A and MEN2B. Science 267:381–383
66. **Chen LC, Kurisu W, Ljung BM, Goldman ES, Moore DI, Smith HS** 1992 Heterogeneity for allelic loss in human breast cancer. J Natl Cancer Inst 84: 506–510
67. **Deng G, Lu Y, Zlotnikov G, Thor AD, Smith HS** 1996 Loss of heterozygosity in normal tissue adjacent to breast carcinomas. Science 274:2057–2059
68. **Wolman SR, Heppner GH** 1992 Genetic heterogeneity in breast cancer. J Natl Cancer Inst 84:469–470